Proceedings of IMECE'04
2004 ASME International Mechanical Engineering Congress and RD&D Expo
November 13-19, 2004, Anaheim, California USA

IMECE2004-60703

DESIGN PRINCIPLES AND AERODYNAMICS OF LOW REYNOLDS NUMBER MULTI-STAGE MICROTURBOMACHINERY

Changgu Lee, Selin Arslan, and Luc G. Fréchette*
Columbia University
Department of Mechanical Engineering
500 West 120th Street, New York NY, 10027

ABSTRACT

In this paper, the design process for multi-stage micro scale turbomachinery will be presented, along with CFD predictions of the key aerodynamic performance parameters required in this design process. This work focuses on the unique and unexplored design space defined by the small scale and planar geometries characteristic of MEMS turbopumps, compressors, gas turbines, steam turbines, or other turbomachinery-based microsystems. Correlations are proposed for the loss coefficient, based on laminar flow theory. A critical Reynolds number is also identified (Re_{crit}=200-300), below which adjacent boundary layers merge, inducing a sharp increase in loss and deviation. This imposes practical limits on the miniaturization of such microturbomachinery.

Keywords: Aerodynamics, turbomachinery, low Reynolds number, MEMS.

INTRODUCTION

Over the past decade, there has a been a growing interest and need for miniature energy conversion systems, such as portable power generation for consumer electronics and soldiers, propulsion for micro air vehicles and satellites, flow handling for micro fuel cells and handheld analytical instruments, as well as miniature cooling units for electronics and people. Meeting this need requires the implementation of traditional thermodynamic cycles at small scale, along with the required machinery. Among the core energy conversion technologies common at large scales, compressors, pumps, and turbines are often used to convert fluid power to mechanical power, or vice versa. Rotating turbomachinery is specifically used for its high power density and reliability, as illustrated by its prevalence in the aerospace (aircraft gas turbine engines) and power generation industries (hydroelectric and land-based gas turbine power generation). Since the fabrication of such complex machines at the millimeter scale can however prove to be challenging and expensive, Epstein and Senturia proposed the use of silicon micromachining and other microelectromechanical (MEMS) technologies [1]. Examples of turbomachinery-based Power MEMS projects include the development of micro gas turbine engines [2], [3], micro rocket turbopumps [4], and micro Rankine steam turbines [5].

The objective of the current work consists of creating a knowledge-base for the design and development of microturbomachinery, with special emphasis on radial, multi-stage configurations. Such knowledge is required in order to develop microsystems with high pressure ratio, high power per unit flow rate, and acceptable efficiency. Previous aerodynamic studies of microturbomachinery aimed at predicting the performance of a few specific single-stage microturbomachines [6],[7],[8] and investigating their operation [9]. In contrast, the current work establishes a design basis for *multi-stage* microfabricated turbomachines and further investigates their aerodynamics at low Reynolds numbers.

Design Space for Microturbomachinery

Typically, large scale turbomachines operate at high Reynolds numbers (on the order of 10^6) and exhibit turbulent flow. Micro-scale configurations considered to date are mostly in the low Reynolds number range ($100 < Re < 10{,}000$), suggesting mainly laminar flow and higher viscous losses. Unfortunately, the body of literature on blade passage aerodynamics (such as design correlations) is limited to high Reynolds numbers hence new investigations are required at smaller scales.

Furthermore, the microfabrication approach constrains the designer to non-traditional configurations. Lithography allows precise patterning of the aerodynamic profiles on the surface of a silicon wafer, and these airfoil shapes are then transferred into the silicon substrate by deep reactive ion etching (DRIE). As illustrated in Figure 1, this approach allows the creation of large arrays of well-defined blades that extend from the silicon substrate, which are most amenable to radial flow. An important outcome of this approach is that the flow area, A_f, increase linearly with radius, $A_f=2\pi r*h$, since the blade height, h, is defined during a single etch step and is therefore

* Corresponding author - phone: (819) 821-8000 x2799; e-mail: lucf@alum.mit.edu; Dr. Fréchette is currently Assistant Professor and Canada Research Chair in Power MEMS at Université de Sherbrooke, QC, Canada, while maintaining an adjunct position at Columbia University.

constrained to be uniform. Due to this fabrication approach, each stage operates at a different tangential speed proportional to radius, $U = \Omega \cdot r$, and the blades are constrained to 2D extruded shapes, without twist along the span.

This paper will first describe a design approach for such planar, multi-stage turbomachinery, and then provide empirical correlations based on numerical simulation of microturbomachinery aerodynamics. The paper will also discuss the observed flow behavior and conclude with design guidelines and future work. Throughout, the analytical developments and examples will focus on *turbines*, although the principles apply for compressors as well.

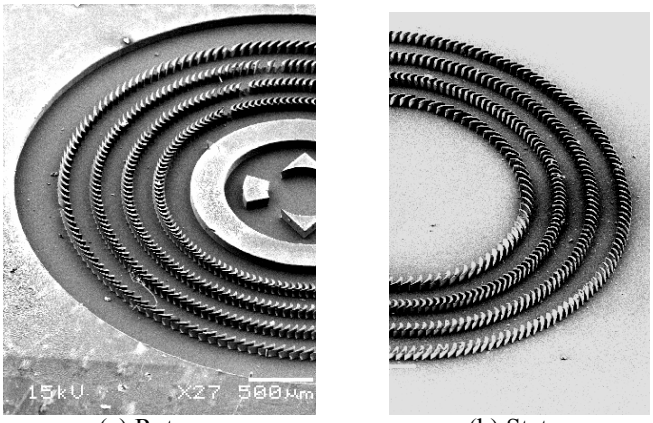

(a) Rotor (b) Stator

(c) Close-up view of a single rotor stage

Figure 1 - SEM image of a typical radial, multi-stage microturbine formed by DRIE, showing the rotors (a) and stators (b) on separate chips, as well as a close-up view of one blade row (c). The turbine is assembled by laying the stator chip over the rotor chip in order to interdigitated the concentric blade rows.

RADIAL, MULTI-STAGE DESIGN APPROACH

The design approach consists of a mean line analysis based on velocity triangles with loss, blockage, and deviation factors. This low order modeling approach is the basis for preliminary design of traditional multi-stage turbomachinery [10]. The flow is however purely radial, through concentric rotor and stator stages of constant blade height. In this paper, flow is considered to be compressible (ideal gas) and adiabatic. The nomenclature used to define the flow velocity components is illustrated in Figure **2**, for a stage composed of a stator and rotor. The process consists of conserving Rothalpy in the relative reference frame of a blade row, conserving mass, applying a loss coefficient correlation to define the relative total pressure, and applying a deviation correlation to define the relative exit flow angle.

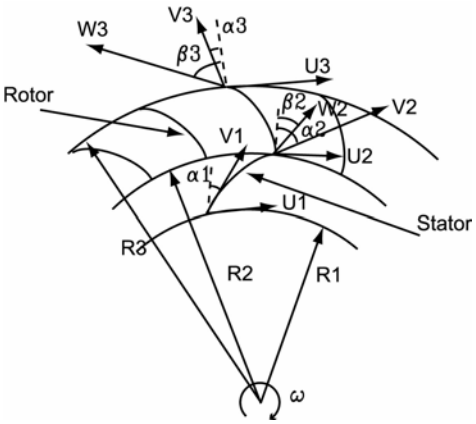

Figure 2 – Velocity triangles in one turbine stage

The pressure loss coefficient for a turbine stator is defined as:

$$Y_N = \frac{P_{01} - P_{02}}{P_{02} - P_2}, \quad Y_N (P_{02} - P_2) = P_{01} - P_{02} \tag{1}$$

where the subscripts represent: 1 inlet, 2 exit, and 0 total property in the stationary frame. At the exit, the isentropic relation in compressible flow is:

$$\frac{P_{02}}{P_2} = (1 + \frac{k-1}{2} M_2^{\,2})^{\frac{k}{k-1}} = C_2, \quad P_{02} = C_2 P_2 \tag{2}$$

where the Mach number is determined from mass conservation at the exit based on the flow area. For mass conservation calculations, the density and mass flow rate are assumed at first. The exit velocity is calculated from mass conservation using velocity triangles to define the flow angles. The relative exit flow angle is defined as the blade angle plus deviation. The exit temperature is determined from energy conservation based on,

$$T_2 = T_1 + \frac{1}{2C_p} V_1^{\,2} - \frac{1}{2C_p} V_2^{\,2} \tag{3}$$

When Eq. (2) is substituted into Eq. (1), the static pressure at the exit is expressed as a function of the inlet total pressure and the loss coefficient.

$$P_2 = \frac{P_{01}}{\{Y_N (1 - 1/C_2) + 1\} C_2} \tag{4}$$

Using the ideal gas relation,

$$P_2 = \rho_2 R T_2 \tag{5}$$

Pressure in Eq. (4) and Eq. (5) can be equated,

$$\rho_2 R T_2 = \frac{P_{01}}{\{Y_N (1 - 1/C) + 1\} C} \tag{6}$$

An iterative approach is then used, by changing the exit density until Eq. (6) is satisfied.

In the rotating frame, which corresponds to the rotor, the total property 0 is replaced by 0w, which is total property in the

rotating frame, V is replace by W, which is the relative velocity, and Y_N by Y_R, which is the loss coefficient in the rotor. Also, in Eq. (2) and Eq. (3), centrifugal terms are added to satisfy Rothalpy conservation in the rotating frame [11], leading to:

$$\frac{P_{02w}}{P_2} = \left(1 + \frac{k-1}{2}\left(M_{2w}^2 - M_{2U}^2\right)\right)^{\frac{k}{k-1}} = C_{2w} \qquad (2)'$$

$$T_2 = T_1 + \frac{1}{2C_p}W_1^{\,2} - \frac{U_1^{\,2}}{2C_p} - \left(\frac{1}{2C_p}W_2^{\,2} - \frac{U_2^{\,2}}{2C_p}\right) \qquad (3)'$$

where M_{2U} is the Mach number based on the wheel speed U_2. The process to find the exit condition in the rotor is the same as the stator except for the above replacements.

Through this process, all the exit conditions are calculated for the assumed flow rate, which is the same through all stages. The flow rate is adjusted by iteration until the exit static pressure at the final stage matches the desired value.

Stage Matching

For a turbine, work should be extracted from each stage with a similar loading distribution. Since the current radial configuration results in flow area and tangential speed that increase linearly with radius, proper flow angle matching at each stage is challenging. A baseline 6-stage microturbine was used to illustrate this aspect, with results of stage output power as a function of rotating speed shown in Figure 3. For the same geometry, incompressible flow calculations suggest that the last stages add work to the flow instead of extracting power, whereas the compressible flow calculations show well matched stages, at a specific operating speed. This large difference is due to expansion of the working fluid in the compressible calculations, since decreasing pressure with radius leads to decreasing density. With the proper radial location of each stage, the density decrease can directly compensate for the through flow area increase and lead to constant radial velocities in all stages. High velocities and hence power densities can therefore be maintained throughout the turbomachine. The desired layout should be such that the radius ratio between two locations is the inverse of the density ratio between those locations: $r_1/r_2 = \rho(r_2)/\rho(r_1)$. Unfortunately, this condition can only be satisfied at one design point, since the density ratio varies with the pressure ratio, hence with speed (Figure 3b).

For a baseline mass flow of 24 mg/s, a power level of 1W per stage is expected, which corresponds to 40 kJ/kg. In order to match the specific power levels defined in the cycle analysis of a Rankine steam turbine, 10 to 30 stages are expected to be required [5]. It is difficult however to match more than 5 stages on a single rotor, so a single rotor is expected to provide on the order of 5 W of mechanical power (200 kJ/kg). Preliminary designs were also developed for a 28 W (1150 kJ/kg), which consists of five individual rotors in series with power levels ranging from 3.8 to 8.4W. It operates with an inlet pressure of 8 MPa and temperature of 780°C.

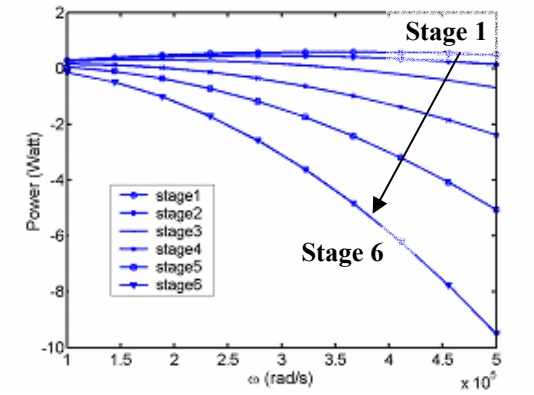

(a) Incompressible flow

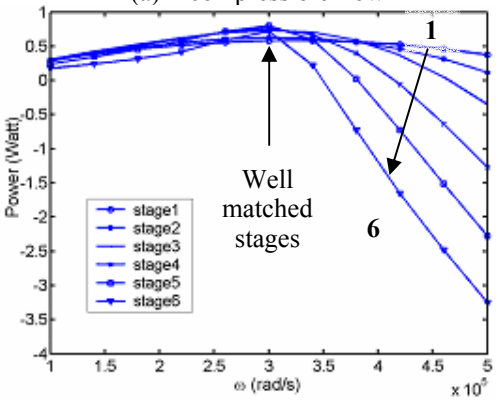

(b) Compressible flow

Figure 3 - Power production per stage for a baseline microturbine (negative power indicated that the stage is adding work to the flow instead of extracting work) – baseline flow rate of 24 mg/s; 2mm diameter rotor.

BLADE PASSAGE AERODYNAMICS

Two main parameters are required as input for the above design process: the loss coefficient and deviation[†]. These aerodynamic parameters depend on the blade passage geometry and operating conditions. The geometry is defined by the airfoil profile, the stagger angle, and the solidity (i.e. the ratio of blade chord to spacing, $\sigma = c/s$). Typically, correlations for loss and deviation are derived from experimental measurements and used in the initial design process. For a given geometry, they are found to depend on the incidence angle and Mach number of the incoming flow, but are not a function of Reynolds number for traditional scale turbomachinery (Re~10^6) [10]. In the operating regimes of microturbomachinery (100<Re<10,000), the influence of Reynolds number is however expected to become important. As a first step, we have therefore chosen to use numerical simulations to explore the flow behavior in microturbomachinery cascades and extract the main performance parameters (loss coefficient and deviation). These will enable the design of experiments to later validate the simulation results. This approach was mainly chosen since the size of microfluidic devices precludes the use of traditional instrumentation and requires the development of embedded sensors, not currently available. Scaled test

[†] Blockage is typically an important design parameter, but it has not been considered to date, since first order estimates of hub and shroud boundary layer thicknesses appear to be negligible with respect to blade height.

apparatus have also been proposed, and exhibit unique experimental challenges [8]. Fortunately at the micro-scale, flows are dominantly laminar and CFD solutions are expected to be increasingly accurate.

The current study is limited to study of loss and deviation as a function of incidence and Reynolds number; the effect of Mach number will be studied subsequently. Two blade passage geometries are considered, as described next.

Blade Passage Geometry

The geometry chosen for this study is based on the NACA A3K7 turbine airfoil [12]. The primary series A3K7 is for reaction blades in which there is acceleration through the cascades. The camber line shape gives rapid turning in the forward part of the blade, where the Mach numbers are low. The profile is defined by a series of points for the camber line (x_c , y_c), and a thickness distribution along that line (with a maximum thickness to chord of t_{max}/c = 20%). The stagger (angle of the blade to the radial direction) and camber (difference between leading and trailing edge angles) are adjusted in order to match the flow angles defined during the previous mean line analysis. Different levels of camber are achieved by scaling the tangential coordinate (x_c , $C \times y_c$) and the blade is tilted to match the incoming flow angle. High camber (Rotor 1) and low camber (Rotor3) blades are analyzed here, with configurations summarized in Table 1. The nominal solidity is $\sigma = 2$. The trailing edge is slightly modified in order to accommodate microfabrication limitations: it is shortened by 2% chord and kept to a minimum thickness of 4 microns.

Table 1 - Blade row configurations

NACA A3K7	Rotor 1	Rotor 3
Chord length	98.29 um	114.76 um
Chord axial	93.07 um	89.33 um
Inlet angle	56°	22°
Outlet angle	-74°	-60°
Stagger	19°	39°

Numerical Simulations

Commercial CFD software (Fluent 6.1) is used for the numerical calculations. The steady-state Navier-Stokes equations are solved for compressible laminar flow through a 2D section of the flow field near mid-span, with adiabatic walls. Blockage due to hub and shroud boundary layers is currently neglected, such that the flow passage is assumed to be of constant effective height (see footnote †). A segregated, implicit solver is chosen with the SIMPLEC pressure-flow coupling algorithm and second order upwind schemes for the energy, momentum, and density equations. Cartesian grids were defined with 27765 nodes (approx. 400X60) for Rotor 1 and 20645 nodes (approx. 320X60) for Rotor 3. The meshes were refined until the main parameter, which is the pressure loss coefficient, does not depend on grid density for given boundary conditions.

The working fluid was air with viscosity defined by Sutherland's law and with the following nominal operating conditions: inlet Mach number M_1 = 0.14, inlet total temperature T_{01}=300K; and exit static pressure P_2 = 1 atm. The inlet static pressure is adjusted to maintain M_1 constant as the incidence or Reynolds number are changed. Calculations were done in a stationary reference frame in order to simulate cascade test conditions. The computational domain was limited to a single blade passage, with inlet and outlet regions extending one chord upstream and downstream respectively.

Effect of incidence

Incidence, defined as the angle between the incoming flow and the blade leading edge, is a key parameter that affects the aerodynamic performance of macro-scale blade rows. The first set of calculations explores the effect of inlet flow angle on the loss coefficient (Eq. 1) and the exit flow angle (i.e. deviation). Numerical results are shown in Figure 4 for both geometries studied here (Rotor 1 and Rotor 3). The exit total pressure and exit flow angle are taken as the mass-average values at the outlet boundary (i.e. one chord downstream of the trailing edge); this approach leads to a conservative, mixed-out loss coefficient. During these calculations, the Reynolds number was maintained at Re = 350±20 and the inlet Mach number at M_1=0.14±0.02. Within the blade passage, the Mach number reaches $0.5 < M_{max} < 0.6$.

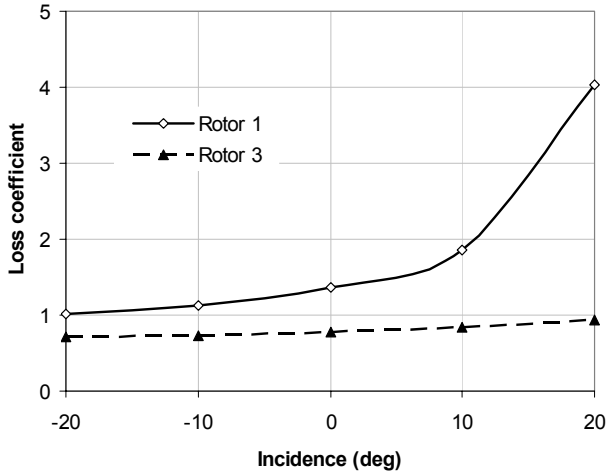

(a) Loss coefficient versus incidence

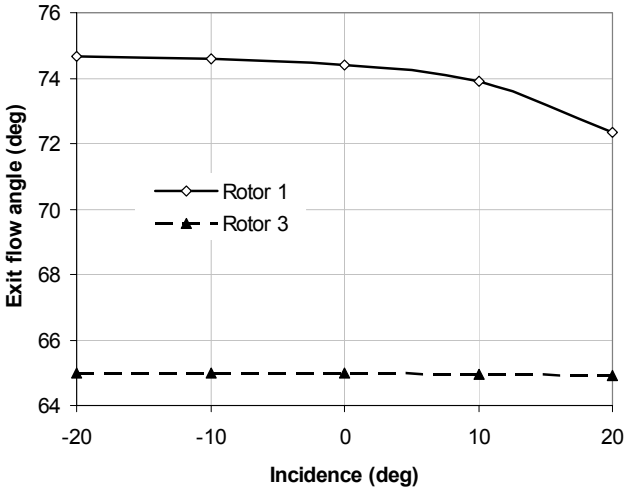

(b) Exit flow angle versus incidence

Figure 4 - Loss coefficient (a) and exit flow angle (b) as a function of incidence for high camber (Rotor 1) and low camber (Rotor 3) NACA A3K7 airfoils, with solidity σ=2. In all cases *Re*=350±20 and inlet Mach number M_1=0.14±0.02.

The main observations in Figure 4 are the increase in loss coefficient and reduction in flow turning with increasing incidence. The effect is most important for the high camber blade row (Rotor 1), whereas the low camber blade row (Rotor 3) remains practically unaffected. Unlike high Re turbomachinery which exhibits flow separation at high positive or negative incidence angles, flow separation was not present in the low Re simulations. Negative incidences even slightly reduced the loss coefficient instead of increasing it.

Effect of Reynolds Number

The second set of calculations explored the effect of Reynolds number on the loss coefficient and the exit flow angle. Numerical results are shown in Figure 5. During these calculations, the inlet Mach number was maintained at M_1=0.14±0.02 and the incidence was fixed to zero. The Reynolds number was varied by scaling the model and changing the inlet total pressure to maintain M_1.

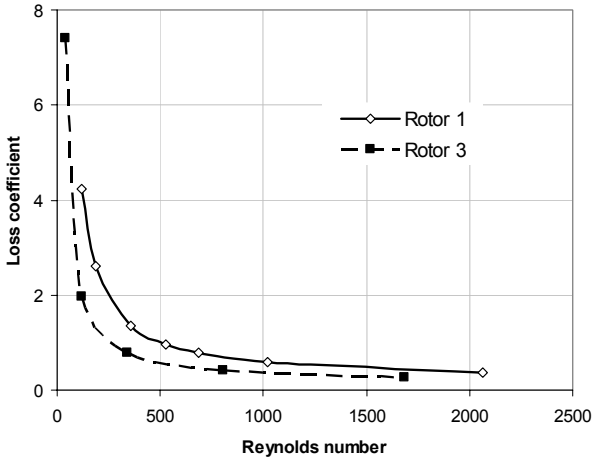

(a) Loss coefficient versus Reynolds number

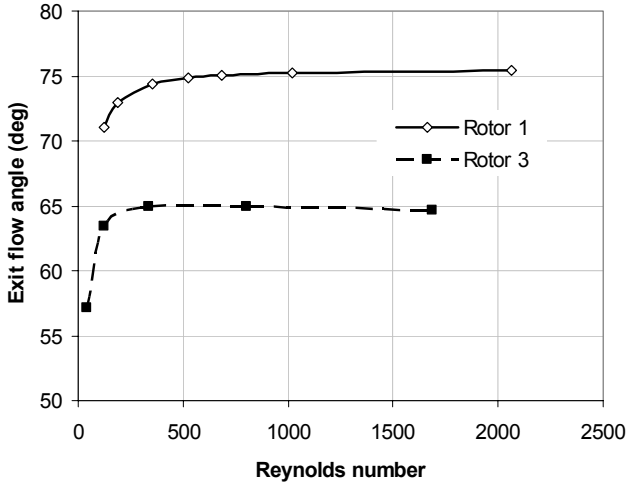

(b) Exit flow angle versus Reynolds number

Figure 5 - Loss coefficient (a) and exit flow angle (b) as a function of Reynolds number for high camber (Rotor 1) and low camber (Rotor 3) NACA A3K7 airfoils, with σ=2. In all cases incidence *i*=0 and inlet Mach number M_1=0.14±0.01.

The most noticeable trend is the gradual increase in total pressure loss and reduction in flow turning as the Reynolds number is reduced. Below a critical Reynolds number of Re_{crit}=200-300, the loss coefficient and deviation start to increase dramatically. This behavior will be discussed later, but it should be noted that no flow separation was observed. As the Reynolds number increases, the loss coefficient and exit flow angle tend to asymptote and therefore become less a function of Reynolds number, as expected.

For design purposes, the following loss coefficient correlation is proposed:

$$Y = \frac{C_1}{\sqrt{\mathrm{Re}}} + \frac{C_2}{\mathrm{Re}} \qquad (7)$$

The first term is inspired from the drag of a laminar boundary layer over a semi-infinite flat plate, while the second term stems from the consideration of the finite plate or airfoil length [13]. By fitting this expression to the numerical results, the following coefficients are found for the specific conditions listed in the previous sections: a) Rotor 1: C_1=6, C_2=400; b) Rotor 3: C_1=6, C_2=170. In general, the coefficients (C_1, C_2) will depend on blade geometry (profile, camber, solidity) and operating conditions (incidence and Mach number).

DISCUSSIONS

Critical Reynolds Number

The critical Reynolds number Re_{crit}=200-300 identified above appears to stem from the change in flow profile at the exit of the blade row, going from boundary layer flow to fully developed flow as the Re decreases. Total pressure contours are shown in Figure 6 for two operating conditions: (a) $Re<Re_{crit}$ and (b) $Re>Re_{crit}$ to illustrate the boundary layer development along the blade passage. As better shown in Figure 7, the velocity magnitude profile across the blade passage at the trailing edge (from suction to pressure side) shifts from core flow at high *Re* to merged boundary layers at low *Re*. This change in regime appears to be associated with increased loss and reduced flow turning.

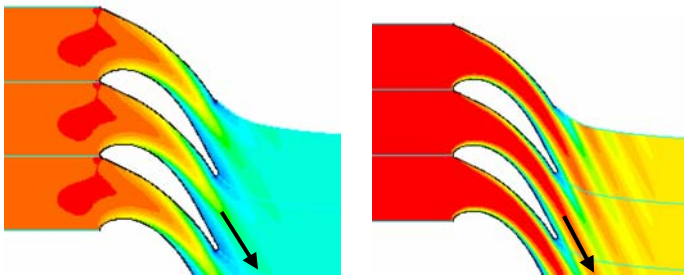

(a) Re = 60 (b) Re = 665

Figure 6 - Total pressure contours for NACA A3K7 turbine stage with solidity of 2 (Rotor 3), showing that low Reynolds numbers (a) lead to thick boundary layers and slightly shallower exit flow angles.

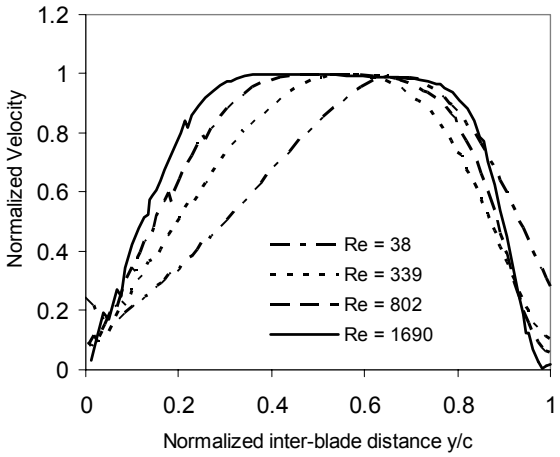

Figure 7 - Profile of normalized velocity magnitude (V/V_{max}) across the flow passage (Rotor 3), taken at 5% chord downstream of the blade row.

A first-order estimate of the critical Reynolds number can be derived from laminar flow relations. First, considering the Blasius solution for laminar flow over a flat plate (with no pressure gradient), the boundary layer thickness at the trailing edge can be defined as [13]:

$$\delta_c = 5.0\sqrt{\frac{\nu\, c}{U_1}} = \frac{5.0\, c}{\sqrt{\mathrm{Re}}} \tag{8}$$

Since the boundary layers will merge at the trailing edge when $\delta_c = s/2$ and solidity is defined as $\sigma = c/s$, we can solve for Re:

$$\mathrm{Re}_{crit,1} = 100\ \sigma^2 \tag{9}$$

For the current configurations, $\sigma = 2$, hence $Re_{crit,1} = 400$. A similar estimate can be done by considering the blade passage as a channel, and defining the Re required such that the entry length, x_{entry}, is equal to the blade chord, c [13]:

$$\frac{x_{entry}}{D} = \frac{c}{s} = 0.04\frac{U_1 D}{\nu} = 0.04\frac{U_1 c}{\nu}\frac{s}{c} = 0.04\frac{\mathrm{Re}}{\sigma} \tag{10}$$

Hence,

$$\mathrm{Re}_{crit,2} = 25\,\sigma^2 \tag{11}$$

and $Re_{crit,2} = 100$ for $\sigma = 2$. These values appear to bound Re_{crit}=200-300 found from the numerical simulations. Based on these observations, one can suggest the following correlation for the critical Reynolds number:

$$\mathrm{Re}_{crit} = 60\,\sigma^2 \tag{11}$$

Effect of solidity

The above expressions suggest that blade rows of higher solidity would incur higher losses and deviation at low Reynolds number. Figure 8 illustrates this point by superposing results for σ=2 and σ=2.5. We can observe a ratio of approximately $(2.5/2)^2$~1.5 between the Re_{crit} (i.e. knee of the curve) for both solidities.

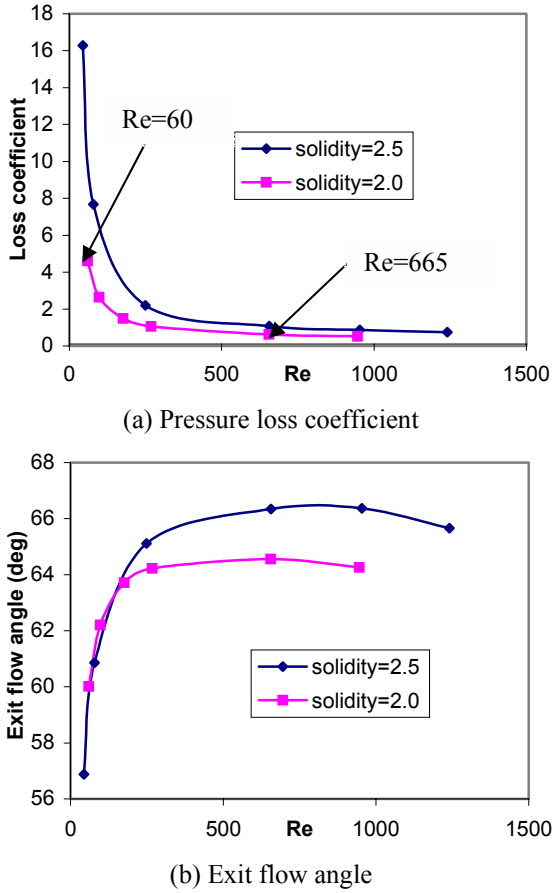

(a) Pressure loss coefficient

(b) Exit flow angle

Figure 8 - Loss coefficient and exit flow angle as a function of Reynolds number for the same airfoil (Rotor 3) but with different solidities, σ = c/s.

CONCLUSIONS

In this paper, we have presented an approach and guidelines for the design of radial, multi-stage microturbomachinery of constant blade height. The main aerodynamic parameters required for the design process (loss coefficient and deviation) were defined using computational fluid dynamics of laminar flow through standard blade profiles, but in the low Reynolds number range. Empirical correlations for the loss coefficient are proposed. It was also found that dramatic increases in loss and deviation occur below a critical Reynolds number of approximately Re_{crit}=200-300. This behavior is associated with merging of the boundary layers at the exit of the blade passage. To maintain acceptable efficiency, it is therefore preferable to limit the scale of microturbomachinery beyond a threshold. For high speed operation, blade chords should be kept above 30-100 microns. At smaller scales, alternate operating principles or configurations should be envisioned.

More extensive studies remain necessary in order to generalize the correlations to account for camber and Mach number. The effects of heat transfer and of inertial forces in the rotating reference frame should also be considered since there are expected to be significant in high speed micro gas turbine and steam turbine engines. Experimental validation is on-going through the fabrication and testing of a 4-stage microturbine as the core component of a micro Rankine steam power generator.

ACKNOWLEDGMENTS

This work was supported by the NASA Glenn Research Center, Alternate Fuels Foundation Technologies program (contracts NAS3-02118 and NAS3-03105), monitored by Dr. Glenn Beheim. The authors gratefully acknowledge this support.

REFERENCES

[1] Epstein A.H. and Senturia S.D., 1997, "Macro Power from Micro Machinery", Science, **276**, p.1211.

[2] Epstein, A.H., et al. 1997, "Micro-Heat Engines, Gas Turbines, and Rocket Engines - The MIT Microengine Project," AIAA Paper 97-1773, *28th AIAA Fluid Dynamics Conference*, Snowmass Village.

[3] Isomura, K., Murayama, M., Yamaguchi, H., Ijichi, N., Asakura, H., Saji, N., Shiga,O., Takahashi, K., Tanaka, S., Genda, T., Esashi, M., 2002, "Development of Microturbocharger and Microcombustor for a Three-Dimensional Gas Turbine at Microscale," *ASME IGTI 2002 TURBO EXPO*, Paper GT-2002-30580, Amsterdam, Netherlands, June 6.

[4] London, A.P., Epstein, A. H., Kerrebrock, J. L., 2001, "High-Pressure Bipropellant Microrocket Engine," *AIAA J. Propulsion and Power*, vol. 17, no. 4, pp. 780-787.

[5] Fréchette, L.G., Lee, C., Arslan, S., Liu, Y.-C., "Design of a Microfabricated Rankine Cycle Steam Turbine for Power Generation", Proc. ASME Int'l Mech. Eng. Congress & Expo., Wash., D.C., Nov. 16-21, 2003.

[6] Mehra, A., 1997, *Computational Investigation and Design of Low Reynolds Number Micro-Turbomachinery*. S.M. Thesis, Massachusetts Institute of Technology, Cambridge, MA.

[7] Jacobson, S.A., 1998, "Aerothermal Challenges in the Design of a Microfabricated Gas Turbine Engine," AIAA paper 98-2445, 29th Fluid Dynamics Conference, Albuquerque, NM.

[8] Shirley, G., 1998, *An Experimental Investigation of a Low Reynolds Number, High Mach Number Centrifugal Compressor*. S.M. Thesis, Massachusetts Institute of Technology, Cambridge, MA.

[9] Fréchette, L.G., Jacobson, S. A., Ehrich, F.F., Ghodssi, R., Khanna, R., Wong, C.W., Zhang, X., Lin, C.-C., Schmidt, M.A., Epstein, A.H., 2004, "High-Speed Microfabricated Silicon Turbomachinery and Fluid Film Bearings". *IEEE/ASME J. Microelectromechanical Systems*, vol. 13, no 6.

[10] Kerrebrock, J.L., 1992, *Aircraft Engines and Gas Turbines*, 2nd Ed., The MIT Press, Cambridge, Massachusetts, pp478.

[11] Greitzer, E.M., Tan, C.S., Graf, M.B., 2004, *Internal Flow: Concepts and Applications*, Cambridge University Press, pp736.

[12] Dunavant, J. C., and Erwin, J. R., 1956, "Investigation of a Related Series of Turbine Blade Profiles in Cascades", NACA Tech. Note 3802.

[13] Schlichting, H., 1979, *Boundary-Layer Theory*, 7th Ed., McGraw Hill, New York, pp817.